IEEE Access
Multidisciplinary | Rapid Review | Open Access Journal

Received February 28, 2018, accepted April 2, 2018, date of publication April 17, 2018, date of current version May 2, 2018.

Digital Object Identifier 10.1109/ACCESS.2018.2823721

Time-Domain Power Quality State Estimation Based on Kalman Filter Using Parallel Computing on Graphics Processing Units

RAFAEL CISNEROS-MAGAÑA[1], (Member, IEEE), AURELIO MEDINA[1], (Senior Member, IEEE), VENKATA DINAVAHI[2], (Senior Member, IEEE), AND ANTONIO RAMOS-PAZ[1], (Member, IEEE)

[1]División de Estudios de Posgrado, Facultad de Ingeniería Eléctrica, Universidad Michoacana de San Nicolás de Hidalgo, Morelia 58030, México
[2]Department of Electrical and Computer Engineering, University of Alberta, Edmonton, AB T6G 2V4, Canada

Corresponding author: Rafael Cisneros-Magaña (rcisneros@dep.fie.umich.mx)

The work of R. Cisneros-Magaña and A. Medina was supported by CONACYT.

ABSTRACT A methodology is developed to assess the time-domain power quality state estimation (PQSE) in electrical systems based on the Kalman filter implemented using parallel processing techniques through graphics processing units (GPUs) to reduce the execution time. The measurements used by the state estimation algorithm are taken from the simulation and transient propagation response of the power network. The parallel Kalman filter (PKF) state estimation obtains the waveforms for busbar voltages and line currents with several sources of time-varying electromagnetic transients. The PKF is evaluated using the compute unified device architecture (CUDA) platform and the CUDA basic linear algebra subprograms library, the parallel filter is executed on GPU cards. Case studies are applied to solve the time-domain state estimation using the proposed PKF-PQSE method, obtaining an execution time reduction and including time-varying harmonics, short circuit faults, and load transient conditions. The speed-up depends on the number of state variables modeling the electrical system under analysis. The PKF-PQSE results are successfully compared and validated against the power systems computer aided design/electromagnetic transients including direct current simulator.

INDEX TERMS Electromagnetic transients, Kalman filters, parallel processing, power quality, state estimation.

I. INTRODUCTION

The PQSE determines the power quality indices during the electrical system operation through simulations, modeling, and measurements. It assesses the dynamic system operation through the time-domain state estimation [1]–[5]. In this contribution, as novelty, the state estimation is solved using the PKF [6]–[8]. The PKF algorithm is programmed using the CUDA platform [9], [10] and the CUBLAS library [11], [12] in graphics processing units (GPU). This parallel algorithm is applied to estimate time-varying electromagnetic transients, harmonics, inter-harmonics, and sub-harmonics distortion. Transient conditions may be present in voltage and current waveforms, which can be accurately obtained through time-domain state estimation assessment. The power system modeling can be replicated through scale-down network prototypes to examine the dynamic operation performance of large-scale systems; the execution time can be significantly reduced using parallel processing techniques. The main contribution of this research work is the proposal of an alternative parallel processing methodology to efficiently solve the PQSE based on GPUs to reduce the execution time and to implement a real-time state estimation tool in power system operation analysis.

In [13]–[15], time-domain state estimation is evaluated using a network model and accounting for noisy measurements from the power system. Modeling, network parameters, measurement points, and electrical quantities to be monitored are important issues to be considered. The signals are sampled and analogue/digital converted; the sampling frequency is associated with the number of points per cycle in the discrete-time solution, thus the measurements must be synchronized. This measurement synchronism can be obtained by the time stamping through the global positioning system (GPS) [1]. A determined number of complete cycles are measured and synchronized, and then these measurements are sent to a control center to process the state estimation

assessment. The discrete waveforms of measurements are the input data to the time-domain PQSE.

In [16], the time-domain harmonic state estimation has been addressed using the PKF, which is now extended to PQSE including the transient state estimation (TSE) to analyze effects such as the short circuit faults, generation changes, and load transients. In this work, the harmonics estimation is examined under a time-varying transient condition.

The time-domain state estimation tracks down fluctuations in the waveforms through the PKF using the criterion of minimize the error between the measurements and their estimated values [17], [18]. The time-varying nature of the electrical generation and load can originate power system transients [19], [20]. It is important to locate and mitigate the transient sources to enhance the power quality indices. This can be achieved with the PQSE to estimate the transients in the power system [21].

Sensors and monitors are required to have a convenient network observability and high speed state estimators to correctly operate and control the power system with safety. The time-domain state estimation demands reliable measurement instrumentation, high-speed communication links, and computer systems with enough memory and adequate numerical processing speed to solve the state estimation [1]. Parallel processing techniques can be applied to considerably reduce the state estimation execution time [22], in particular, when the order of related matrices is significantly large and the associated operations can be simultaneously conducted [23]–[26].

Heterogeneous programming executes the sequential parts of algorithms in the CPU cores and the steps feasible of being parallel programmed are processed on GPUs [27]. CUDA is a hardware-software platform from Nvidia; it can be applied to run the parallel programs using the C++ language; these programs include special commands which are executed in the GPU hardware [9]. The CPU or host computes the sequential parts of a determined algorithm to be evaluated while the parts suitable to be processed in parallel form are executed in the GPU or device using kernels, i.e. the parallel functions of the GPU. During the kernel execution, blocks are created with an equal number of threads to run the parallel function. Blocks of threads form a grid [10], [27], and the GPUs act as coprocessors of the CPU. The CUBLAS library is the parallel version of the basic linear algebra subprograms (BLAS) library. The CUBLAS functions assess the vector and matrix operations of linear algebra in GPUs through parallel processing techniques and the CUDA architecture [11].

An important issue of parallel programming on GPUs is the necessary data exchange between the CPU and the GPU. This data flow takes time being part of the parallel program. The data flow between the CPU and GPU should be minimized by first allocating the necessary data to decrease the PKF execution time. Data are numerically processed in parallel; the results are saved back to the CPU and the GPU memory is cleared once the time of analysis is completed [11], [12].

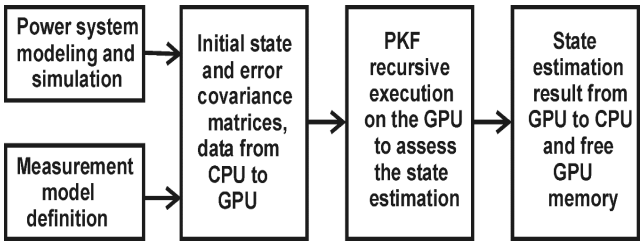

FIGURE 1. PQSE based on KF using parallel computing on CPU-GPU systems.

The rest of paper is organized as follows: Section 2 presents the proposed PKF-PQSE methodology to solve the time-domain state estimation. Section 3 includes the case studies associated with variable harmonics, inter-harmonics, sub-harmonics, and electromagnetic transients. Section 4 refers to the CPU-GPU characteristics and the involved execution time for the analyzed case studies, and Section 5 draws the main conclusions of this research work.

II. METHODOLOGY

The PKF obtains the time-domain state estimation by performing the following procedure steps:

a) System and measurement models definition and power system simulation.

b) Initial condition and data allocation in GPU memory.

c) PKF recursive execution in GPU.

d) Save the state estimation results.

e) Clear GPU memory after case study ending.

These steps are illustrated in Fig. 1.

The power system can be modeled in the state-space framework through a first-order ordinary differential equation (ODE) set, i.e.

$$d\boldsymbol{x}/dt = \boldsymbol{A}\boldsymbol{x} + \boldsymbol{B}\boldsymbol{u} \tag{1}$$

$$\boldsymbol{y} = \boldsymbol{C}\boldsymbol{x} + \boldsymbol{D}\boldsymbol{u} \tag{2}$$

The continuous-time model can be converted to discrete-time model. To this purpose, the differential equations are approximated by difference equations [28], by assuming the direct transmission matrix $\boldsymbol{D}$ equal to zero, the discrete model is given as,

$$\boldsymbol{x}_{k+1} = \boldsymbol{A}_{\boldsymbol{d}}\boldsymbol{x}_k + \boldsymbol{B}_{\boldsymbol{d}}\boldsymbol{u}_k \tag{3}$$

$$\boldsymbol{y}_k = \boldsymbol{C}\boldsymbol{x}_k \tag{4}$$

Where $\boldsymbol{x}$ is the state vector, $\boldsymbol{A}_{\boldsymbol{d}}$ the discrete state transition matrix, $\boldsymbol{B}_{\boldsymbol{d}}$ the discrete input matrix, $\boldsymbol{u}$ the input vector, $\boldsymbol{y}$ the output vector, $\boldsymbol{C}$ the output matrix; $\boldsymbol{A}_{\boldsymbol{d}}$ and $\boldsymbol{B}_{\boldsymbol{d}}$ can be obtained using the Taylor's series expansion,

$$\boldsymbol{A}_{\boldsymbol{d}} = \exp(\boldsymbol{A}t) \approx \boldsymbol{I} + \boldsymbol{A}t + \boldsymbol{A}t^2/2 \tag{5}$$

$$\boldsymbol{B}_{\boldsymbol{d}} = \int_0^t e^{\boldsymbol{A}\xi}\boldsymbol{B}d\xi \approx \boldsymbol{B}t + (\boldsymbol{A}\boldsymbol{B}t)^2/2 \tag{6}$$

If the time step is small, (5) and (6) can be approximated by,

$$\boldsymbol{A}_{\boldsymbol{d}} \approx \boldsymbol{I} + \boldsymbol{A}t \approx \boldsymbol{\Phi} \tag{7}$$

$$\boldsymbol{B}_{\boldsymbol{d}} \approx \boldsymbol{B}t \tag{8}$$

$\boldsymbol{A_d}$ is the state transition matrix; it is also represented by Φ, thus the discrete model is defined as,

$$\boldsymbol{x}_{k+1} = \boldsymbol{\Phi x}_k + \boldsymbol{B_d u}_k + \boldsymbol{v}_k \quad (9)$$

$$\boldsymbol{y}_k = \boldsymbol{C x}_k + \boldsymbol{w}_k \quad (10)$$

The noise terms, $\boldsymbol{v}$ the process noise, and $\boldsymbol{w}$ the measurement noise, are added to (9) and (10), respectively. They are usually considered stationary, Gaussian, with zero mean value, and uncorrelated.

$$\boldsymbol{v}_k \approx N(0, \boldsymbol{Q}_k) \quad (11)$$

$$\boldsymbol{w}_k \approx N(0, \boldsymbol{R}_k) \quad (12)$$

The process and measurement noise covariance matrices are represented by $\boldsymbol{Q}$ and $\boldsymbol{R}$, respectively.

The system dynamics is described by (1) and (9), while the measurement state estimation equation is related to (2) and (10) as,

$$z_k = \boldsymbol{H x}_k + \boldsymbol{e}_k \quad (13)$$

where $\boldsymbol{z}$ is the measurement vector; this vector contains the output variables selected as measurements from vector $\boldsymbol{y}$, $\boldsymbol{H}$ is the measurement state estimation matrix. This matrix describes the relationship between state variables and measurements, and $\boldsymbol{e}$ is the state estimation error, which represents the difference or residual between the actual or real measurement values and the estimated measurements.

The KF algorithm begins by considering an initial condition for the state vector; this condition can be assumed equal to zero, $\boldsymbol{x}(0)$=0. The initial error covariance matrix is defined as,

$$\boldsymbol{P}(0) = \boldsymbol{E}\left[\left(\hat{\boldsymbol{x}} - \boldsymbol{x}(0)\right)\left(\hat{\boldsymbol{x}} - \boldsymbol{x}(0)\right)^T\right] = \boldsymbol{E}[\left(\hat{\boldsymbol{x}}\right)\left(\hat{\boldsymbol{x}}\right)^T] \quad (14)$$

where $\boldsymbol{E}$ is the expected value.

The recursive KF algorithm can be divided into three main steps [6], as:

1. A priori time update.

1.1 Predict state vector.

$$\bar{\boldsymbol{x}}_{k+1} = \boldsymbol{\Phi}_k \hat{\boldsymbol{x}}_k + \boldsymbol{B_d u}_k \quad (15)$$

1.2 Predict error covariance matrix.

$$\bar{\boldsymbol{P}}_{k+1} = \boldsymbol{\Phi}_k \boldsymbol{P}_k \boldsymbol{\Phi}_k^T + \boldsymbol{Q}_k \quad (16)$$

2. KF gain.

$$\boldsymbol{K}_{k+1} = \bar{\boldsymbol{P}}_{k+1} \boldsymbol{H}^T (\boldsymbol{H} \bar{\boldsymbol{P}}_{k+1} \boldsymbol{H}^T + \boldsymbol{R}_k)^{-1} \quad (17)$$

3. Measurement update.

3.1 Update state vector.

$$\hat{\boldsymbol{x}}_{k+1} = \bar{\boldsymbol{x}}_{k+1} + \boldsymbol{K}_{k+1}(z_{k+1} - \boldsymbol{H} \bar{\boldsymbol{x}}_{k+1}) \quad (18)$$

3.2 Update error covariance matrix.

$$\boldsymbol{P}_{k+1} = (\boldsymbol{I} - \boldsymbol{K}_{k+1} \boldsymbol{H}) \bar{\boldsymbol{P}}_{k+1} \quad (19)$$

$\boldsymbol{Q}$ and $\boldsymbol{R}$ matrices are the process and measurement noise covariance matrices, associated with $\boldsymbol{v}$ and $\boldsymbol{w}$ noises, respectively. These matrices are defined by,

$$\boldsymbol{Q}_k = \boldsymbol{E}(\boldsymbol{v}_k \boldsymbol{v}_k^T) \quad (20)$$

$$\boldsymbol{R}_k = \boldsymbol{E}(\boldsymbol{w}_k \boldsymbol{w}_k^T) \quad (21)$$

The inverse matrix of (17) can be obtained through LU decomposition with backward-forward substitutions. These numerical processes can be parallel executed using the CUBLAS functions in the GPU. The LU decomposition can be based on the Crout's reduction algorithm [29], [30]. For a $\mathbb{R}^{m \times m}$ square matrix, the steps of this algorithm are as follows:

a) Subdivide the matrix to invert to define the first element as pivot,

$$\boldsymbol{A} = \begin{bmatrix} a_1 & \boldsymbol{A}_H \\ \boldsymbol{A}_V & \boldsymbol{A}_2 \end{bmatrix} \quad (22)$$

where a_1 is the pivot, $\boldsymbol{A}_V \in \mathbb{R}^{(m-1)\times 1}$, $\boldsymbol{A}_H \in \mathbb{R}^{1\times(m-1)}$, and $\boldsymbol{A}_2 \in R^{(m-1)\times(m-1)}$.

b) Multiply $\boldsymbol{A}_V$ by the reciprocal of the pivot as,

$$\boldsymbol{A}'_V = (1/a_1)\boldsymbol{A}_V \quad (23)$$

$$\boldsymbol{A}' = \begin{bmatrix} a_1 & \boldsymbol{A}_H \\ \boldsymbol{A}'_V & \boldsymbol{A}_2 \end{bmatrix} \quad (24)$$

c) Evaluate $A_2{}'$ as,

$$\boldsymbol{A}'_2 = \boldsymbol{A}_2 - (\boldsymbol{A}'_V)\boldsymbol{A}_H \quad (25)$$

d) Substitute $\boldsymbol{A}_2$ in $\boldsymbol{A}'$ (24) by $\boldsymbol{A}_2{}'$ (25) to obtain $\boldsymbol{A}''$ (26) as,

$$\boldsymbol{A}'' = \begin{bmatrix} a_1 & \boldsymbol{A}_H \\ \boldsymbol{A}'_V & \boldsymbol{A}'_2 \end{bmatrix} \quad (26)$$

Equation (26) is the result of the first pivoting. To continue with the next pivot, the first diagonal element of $\boldsymbol{A}'_2$is now the new pivot; the steps a-d are applied to $\boldsymbol{A}'_2$to complete the new pivoting. This pivoting process is repeated from 1 to m-1 times for the diagonal elements of $\boldsymbol{A}$. The result is the $\boldsymbol{U}$ upper triangular matrix and the $\boldsymbol{L}$ unit lower triangular matrix, i.e. the LU decomposition, which is obtained in the same place of the original matrix.

After the LU decomposition, backward-forward substitutions are applied to obtain the inverse matrix. Notice that matrix-vector operations can be carried-out using parallel processing in the GPU.

The normalized root mean square error (NRMSE) is used to validate the proposed methodology. This error measures the difference between estimated values and the values actually observed; lower error indicates less estimation residual. The NRMSE is defined by,

$$NRMSE = \frac{\sqrt{\sum_{t=1}^{np} \frac{(\hat{\boldsymbol{x}}_t - \boldsymbol{x}_t)^2}{np}}}{\boldsymbol{x}_{max} - \boldsymbol{x}_{min}} \quad (27)$$

where $\hat{\boldsymbol{x}}$ is the estimated vector, $\boldsymbol{x}$ is the real or actual vector, and np the number of points.

TABLE 1. Kalman filter matrix and vector order.

Matrix or vector	Order	Description
$\boldsymbol{x}$	$n\times1$	State vector
$\boldsymbol{B}$	$n\times1$	Input matrix
$\boldsymbol{U}$	$i\times1$	Input vector
$\boldsymbol{\Phi}$	$n\times n$	State transition matrix
$\boldsymbol{H}$	$m\times n$	Measurement matrix
$\boldsymbol{P}$	$n\times n$	Error covariance matrix
$\boldsymbol{Q}$	$n\times n$	Process noise covariance matrix
$\boldsymbol{R}$	$m\times m$	Measurement noise covariance matrix
$\boldsymbol{K}$	$n\times m$	Kalman filter gain matrix

When parallel algorithms are evaluated, the main interest is to assess the efficiency with respect to the sequential implementation. The speed-up gives the relative benefit of the parallel solution against the sequential program execution and it is defined as the relation between the time taken to complete the solution using only one processor working in sequential form and the time required to obtain the same solution using several processors working in parallel. If the sequential processor is identical to the parallel processors, the speed-up is defined as,

$$S = T_S/T_P \tag{28}$$

where T_s is the sequential execution time, T_p is the parallel execution time, and S the speed-up [31].

If the sequential processor and the parallel processors have different computational characteristics, a factor f_s is introduced to normalize the speed up as,

$$S_n = S/f_s = T_s/[T_p\,(fs)] \tag{29}$$

where S_n is the normalized speed-up, f_s speed-up factor which depends of the relation between the sequential to parallel computational characteristics [32], [33].

A. KALMAN FILTER BASED ON THE PARALLEL CUBLAS FUNCTIONS

The KF takes the discrete state space modeling represented by (9) and (10), and the measurement model (13), to follow the power system dynamics and to estimate the state and output variables, considering synchronized measurements from the power system that may be contaminated with noise. The KF attempts to separate the measurement and process noises to estimate the state variables [17]. Table 1 gives the order of the associated matrices with i inputs, m measurements, and n states.

The flowchart of Fig. 2 gives the PKF numerical process; all matrix operations are parallel executed in the GPU using the CUBLAS functions.

Table 2 indicates the parallel CUBLAS functions to perform the steps of PKF flowchart shown in Fig. 2. They evaluate vector-vector addition, matrix-vector product, matrix-matrix addition, matrix-matrix product, among other operations; these CUBLAS functions are parallel processed

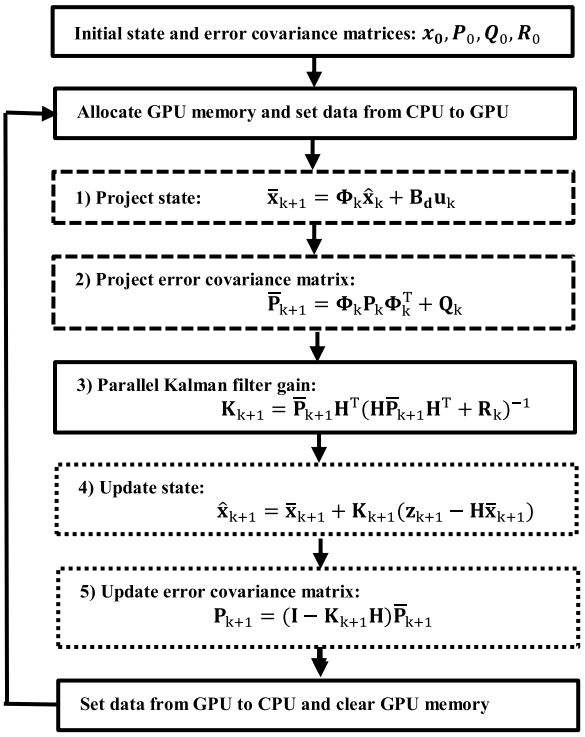

FIGURE 2. KF flowchart, matrix operations are parallel evaluated in the GPU using the CUBLAS functions.

in the GPU using a column vector form to operate all vectors and matrices. Operation vectoring in GPUs reduces the execution time [11], [12].

The inverse matrix in the PKF algorithm (step 3) is obtained using the LU decomposition jointly with backward-forward substitutions. The parallel CUBLAS functions Dscal and Dger are used to obtain the LU factors. They are executed m-1 times (m measurements) to obtain the LU decomposition. These functions assess the Crout's reduction algorithm (22)-(26). The Dtrsm function evaluates the backward-forward substitutions to obtain the inverse matrix of (17) [12]. Step 3 takes most of the PKF execution time with the inverse matrix being calculated at each time-step of the state estimation [34].

Table 1 gives the matrices and vectors that are allocated and set with initial values in the GPU memory. The KF recursive algorithm is in turn executed in the GPU through the parallel CUBLAS functions; the state estimation solution is sent from GPU memory to CPU memory. Transients and harmonics are time-varying effects during the power system operation that can be traced with the KF implemented in parallel execution.

III. POWER QUALITY STATE ESTIMATION CASE STUDIES

The IEEE 14-bus test power system shown in Fig. 3 is evaluated in the case studies to follow. A three-phase 100 MVA base power and a phase–phase 230 kV base voltage are used to obtain the pu values. The transmission lines 1-2, 1-5, 2-3, 2-4, 2-5, 3-4, and 4-5 are represented by the nominal-π circuit line model, and the rest of the lines by a series-impedance; the power transformers 4-9, 5-6, 4-8-9 are modeled by inductive

TABLE 2. Parallel CUBLAS functions to assess the KF steps in Fig. 2 with m measurements.

PKF	Step	Cublas function	Description
1.- Project state	$\boldsymbol{\Phi}_k\hat{\boldsymbol{x}}_k$	Dgemv	matrix-vector product
	$\mathbf{B_d}\boldsymbol{u}_k$	Dgemv	matrix-vector product
	$\overline{\boldsymbol{x}}_{k+1} = \boldsymbol{\Phi}_k\hat{\boldsymbol{x}}_k + \mathbf{B_d}\boldsymbol{u}_k$	Daxpy	vector-vector addition
2.- Project covariance matrix	$\boldsymbol{\Phi}_k\boldsymbol{P}_k$	Dgemm	matrix-matrix product
	$\boldsymbol{\Phi}_k\boldsymbol{P}_k\boldsymbol{\Phi}_k^T$	Dgemm	matrix-matrix product
	$\overline{\boldsymbol{P}}_{k+1} = \boldsymbol{\Phi}_k\boldsymbol{P}_k\boldsymbol{\Phi}_k^T + \boldsymbol{Q}_k$	Dgeam	matrix-matrix addition
3.- KF gain	$\overline{\boldsymbol{P}}_{k+1}\boldsymbol{H}^T$	Dgemm	matrix-matrix product
	$\boldsymbol{H}\overline{\boldsymbol{P}}_{k+1}\boldsymbol{H}^T$	Dgemm	matrix-matrix product
	$\boldsymbol{H}\overline{\boldsymbol{P}}_{k+1}\boldsymbol{H}^T + \boldsymbol{R}_k$	Dgeam	matrix-matrix addition
	$\boldsymbol{LU}$ decomp$(\boldsymbol{H}\overline{\boldsymbol{P}}_{k+1}\boldsymbol{H}^T + \boldsymbol{R}_k)$		LU dec., m-1 times next two functions
		Dscal	scales vector by scalar, eq. (23)
		Dger	vector product & matrix diff., eq. (25)
	$(\boldsymbol{H}\overline{\boldsymbol{P}}_{k+1}\boldsymbol{H}^T + \boldsymbol{R}_k)^{-1}$	Dtrsm	backward substitution
		Dtrsm	forward substitution
	$\boldsymbol{K}_{k+1} = \overline{\boldsymbol{P}}_{k+1}\boldsymbol{H}^T(\boldsymbol{H}\overline{\boldsymbol{P}}_{k+1}\boldsymbol{H}^T + \boldsymbol{R}_k)^{-1}$	Dgemm	matrix-matrix product
4.- Update state	$\boldsymbol{H}\overline{\boldsymbol{x}}_{k+1}$	Dgemv	matrix-vector product
	$\boldsymbol{z}_{k+1} - \boldsymbol{H}\overline{\boldsymbol{x}}_{k+1}$	Daxpy	vector-vector difference
	$\boldsymbol{K}_{k+1}(\boldsymbol{z}_{k+1} - \boldsymbol{H}\overline{\boldsymbol{x}}_{k+1})$	Dgemv	matrix-vector product
	$\hat{\boldsymbol{x}}_{k+1} = \overline{\boldsymbol{x}}_{k+1} + \boldsymbol{K}_{k+1}(\boldsymbol{z}_{k+1} - \boldsymbol{H}\overline{\boldsymbol{x}}_{k+1})$	Daxpy	vector-vector addition
5.- Update covariance matrix	$\boldsymbol{K}_{k+1}\boldsymbol{H}$	Dgemm	matrix-matrix product
	$\boldsymbol{I} - \boldsymbol{K}_{k+1}\boldsymbol{H}$	Dgeam	matrix-matrix difference
	$\boldsymbol{P}_{k+1} = (\boldsymbol{I} - \boldsymbol{K}_{k+1}\boldsymbol{H})\overline{\boldsymbol{P}}_{k+1}$	Dgemm	matrix-matrix product

reactances, according to the IEEE 14 bus test power system specification [35].

The synchronous generators are modeled by sinusoidal voltage sources at the fundamental frequency, inductive electric loads are connected at the indicated busbars. The test power system is modified to include variable harmonic sources connected at busbars 12, 13, and 14 to represent

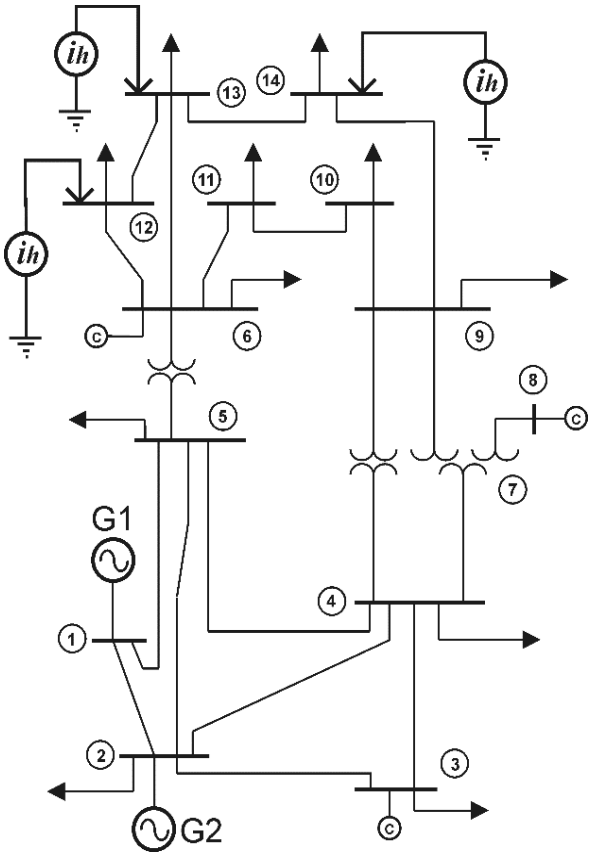

FIGURE 3. Modified IEEE 14-bus test power system including harmonic sources at busbars 12, 13, and 14.

nonlinear electric loads injecting harmonic and interharmonic currents. Under this operating condition, the harmonic and transient state estimation can be assessed through the recursive PKF algorithm [20].

The power system state space model consists of 43 first-order ordinary differential equations (ODE) for a single-phase case. This model is solved to assess the harmonic propagation or a transient condition in the network using the fourth-order Runge-Kutta (RK4) method with a time-step of 512 points per cycle or 32.55 microseconds. Table 3 gives the state variables of the system and the output variables taken as measurements.

The harmonic distortion and transients are estimated using the PKF algorithm including the state space model and the measurement equation $\boldsymbol{z}=\boldsymbol{Hx}$. Second row of Table 3 indicates the states that are selected as measurements to define the $\boldsymbol{z}$ vector. The measurement equation has an underdetermined condition with the 38 selected measurements; the PKF methodology estimates the state variables and attempts to obtain the minimum error between the actual and estimated values.

A. PKF-PQSE INCLUDING TIME-VARYING HARMONIC SOURCES AT BUSBARS 12, 13, AND 14

Table 4 gives time-varying harmonic injections, which can be generated during the operation of power systems when

TABLE 3. State and monitored variables.

Variables	Line current	Busbar voltage	Load current
state variables	1-20	21-32	33-43
measurements	1-15	21-32	33-43

TABLE 4. Time-varying harmonic injections.

Busbars	Cycles	Harmonics	Peak value (A)
12, 13, 14	1-6	5	3.000
		7	1.500
		11	0.750
		13	0.375
	7-10	5	9.000
		7	4.500
		11	2.250
		13	1.125
	11-14	5	15.000
		7	7.500
		11	3.750
		13	1.875

nonlinear electric loads are connected, e.g. motor drives, AC/DC rectifiers, DC/AC inverters, HVDC links, thyristor controlled devices or flexible ac transmission systems (FACTS), among others loads [36]–[40]. The injected harmonics are increased during the last seven cycles to estimate a time-varying harmonic condition. The harmonic magnitudes are increased three times of their initial values during cycles 7-10 and then five times during cycles 11-14 at busbars 12, 13, and 14.

The PKF obtains the harmonic state through the first-order ODE set, modeling the power system, and the available measurements, which can be contaminated with a stationary and Gaussian noise, this noise is assumed as being 2% signal-to-noise ratio (SNR).

A close agreement is obtained between the actual values and the proposed PKF solution. Fig. 4 illustrates the actual and estimated state variables and their difference for line currents. Actual and observed variables are obtained from the harmonic propagation response through the state space model and the fourth-order RK4 method with a time step of 32.55 microseconds.

The difference represents the error between the actual and estimated values. This error presents an increase when the total harmonic distortion is increased, during 7-10 cycles and then during 11-14 cycles. The error increase is due to the fast fluctuations in the waveforms; its maximum magnitude is 4.6%.

Fig. 5 shows the waveforms for generator currents at busbars 1-2 under the time-varying harmonic condition. The generator currents are calculated using the

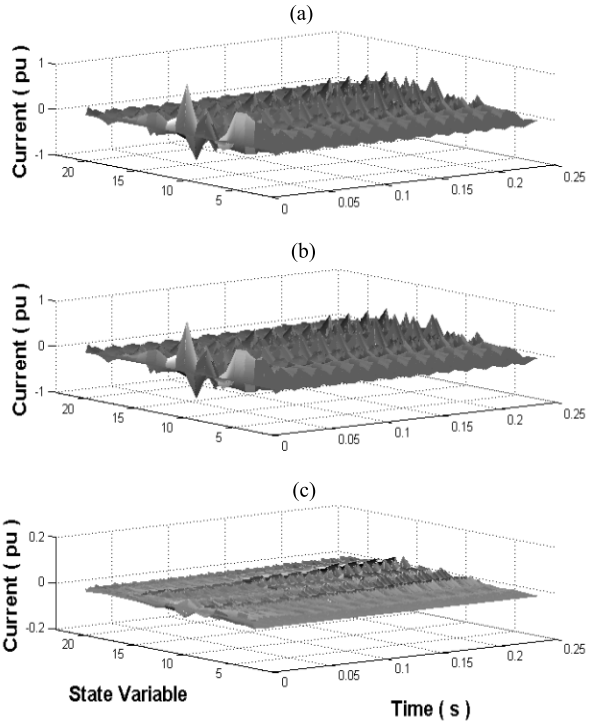

FIGURE 4. Waveforms of line currents, assuming time varying harmonic sources at busbars 12, 13, and 14. (a) Actual, (b) PKF estimate, (c) Difference.

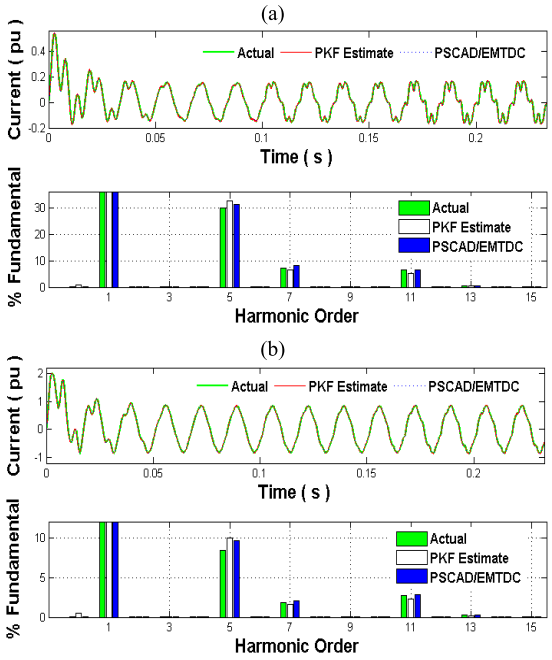

FIGURE 5. Actual, PKF estimation, and PSCAD/EMTDC response with time-varying harmonics. (a) Generator waveform at busbar 1 and harmonic content, (b) Generator waveform at busbar 2 and harmonic content. The estimation is identical to the actual current waveforms.

estimates for the line currents (Fig. 4) and applying the KCL. Actual and PKF estimated waveforms are validated through direct comparison against the power systems computer aided design/electromagnetic transients including direct current (PSCAD/EMTDC) solution. The actual,

TABLE 5. Sub-harmonic and inter-harmonics injections at busbars 12,13, and 14.

Component	Frequency Hz	Magnitude Amp.	Magnitude pu
sub-harmonic	30	18.0	0.072
inter-harmonic 1	90	9.0	0.036
inter-harmonic 2	150	4.5	0.018

estimated and PSCAD/EMTDC waveforms closely agree with the proposed PKF methodology. The NRMSE is 0.92% and 0.53% for the PKF estimates, 0.7% and 0.68% for the PSCAD/EMTDC responses for generator currents at busbars 1 and 2, respectively, as compared against the actual response.

The harmonic content for generator currents is obtained using the discrete Fourier transform (DFT) during the last cycle of the waveforms. For the generator current waveform at busbar 1, THD is 31.2%, 33.6%, and 33.0% for actual, PKF estimate, and PSCAD/EMTDC waveforms, respectively. Similarly, THD is 9.0%, 10.3%, and 10.1% for actual, PKF estimate, and PSCAD/EMTDC waveforms, respectively, for the current of the generator at busbar 2. This harmonic distortion is due to the harmonic currents injected at busbars 12, 13, and 14, which in turn flow through network lines and reach the generators and loads, adversely affecting the power quality and the power system operation.

B. PKF-PQSE INCLUDING SUB-HARMONICS AND INTER-HARMONICS

The inter-harmonics can be present in the distorted waveforms; they have intermediate harmonic frequencies. In general, inter-harmonics rms values are low, as compared against the fundamental frequency rms value. Power quality is affected due to the presence of inter-harmonics, as cause heating, flicker, communications interference, and magnetic saturation, among others [41].

Inter-harmonics can be generated by nonlinear loads such as rectifiers, dc/ac converters, thyristor controlled electronic devices, speed motor drives, and electric arc furnaces, among other nonlinear electrical loads [42].

The injected harmonics at busbars 12, 13, and 14 are added with a sub-harmonic and two inter-harmonic components to review the effect on the line currents and busbar voltages of the test power system using the PKF method. Table 5 gives the frequency and magnitude of these components.

Fig. 6 shows the actual, PKF estimation, and PSCAD/EMTDC waveforms for line currents 6-11 and 7-8. The NRMSE for these currents are 0.85% and 0.81% for PKF estimates; and 0.78% and 0.92% for the PSCAD/EMTDC responses [43], respectively.

The high waveform distortion is generated by the harmonics, sub-harmonic, and inter-harmonics injections. Line 6-11 current has a THD of 30.12%, 30.10%, and 29.59% for actual, PKF estimation, and PSCAD/EMTDC

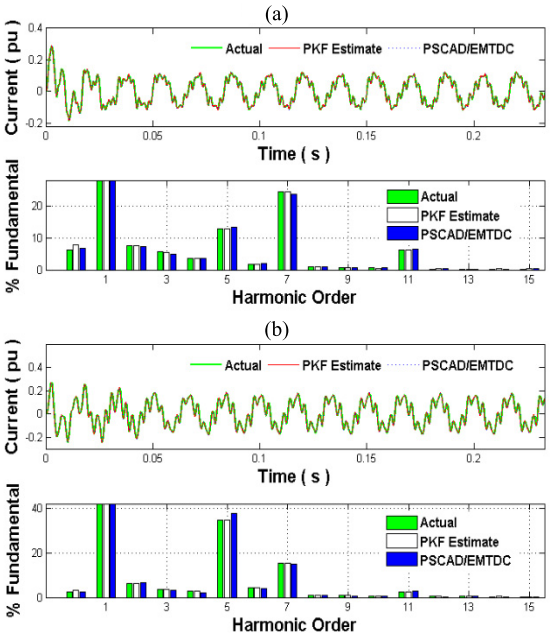

FIGURE 6. PKF-PQSE including harmonics, sub-harmonics, and inter-harmonics injections at busbars 12, 13, and 14. (a) Line current waveform 6-11 and harmonic content, (b) Line current waveform 7-8 and harmonic content. The NRMSE is less than 1%.

response, respectively. For line 7-8 current, THD is 38.92%, 38.95%, and 41.45%, for actual, PKF estimation, and PSCAD/EMTDC, respectively. The maximum difference between solutions is approximately 2.5%.

The waveforms contain dc component and even harmonics; this is due to the injected currents including sub-harmonics, inter-harmonics, and harmonic distortion, which flow from the electric loads through the lines and reach the generators.

Fig. 7 shows the voltage waveform at busbar 8 and its harmonic content; this is one of the most distorted busbar voltages in the network. THD is 10.1%, with particular presence of 3rd, 5th, and 7th harmonics, of 3.5%, 9.3%, and 2.4%, respectively.

The high voltage waveform distortion is again due to the nonlinear load currents represented by the injections of harmonics, inter-harmonics, and sub-harmonics; also, the presence of even harmonics is due to these components.

C. PKF-PQSE WITH A SHORT CIRCUIT FAULT AT BUSBAR 6

A transient condition can be originated by faults, load or generation changes, switching, lighting, among others effects [36]. Transients are estimated using the proposed PKF-PQSE methodology. To this purpose, a single-phase to ground fault is applied at busbar 6 connecting a resistance of 0.52 pu between busbar and ground; beginning at 7th cycle and ending at 9th cycle of the time interval. PKF-PQSE allows the estimation of line currents using noisy and partial measurements from the system. For this case study, 2% of SNR noise is added to measurements.

Fig. 8 shows the waveforms for line currents, state variables 1-20, i.e. actual, PKF-PQSE estimates, and their

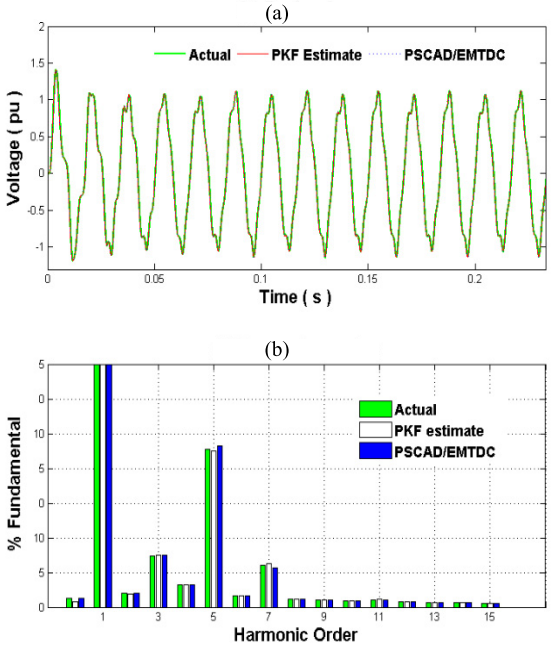

FIGURE 7. Voltage busbar 8 including harmonics, sub-harmonics and inter-harmonics injections at busbars 12, 13, and 14. (a) Waveform, (b) Harmonic content. The THD is 10.1%.

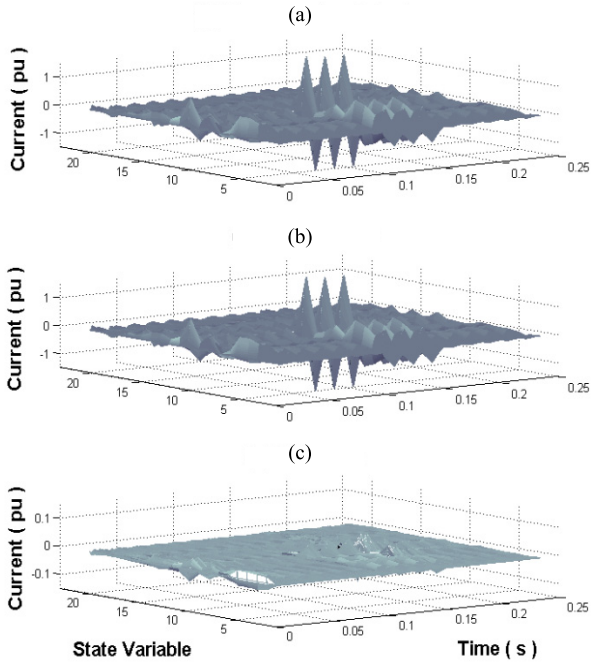

FIGURE 8. Actual, PKF estimation, and difference of line currents, single-phase to ground fault at busbar 6. (a) Actual, (b) PKF estimate, (c) Difference.

difference. Please observe the close agreement achieved between actual and estimated waveforms, with a maximum difference of 2% between responses.

Fig. 9 shows the short circuit transient condition for currents in transformer 5-6, line 6-11, and their residuals; starting

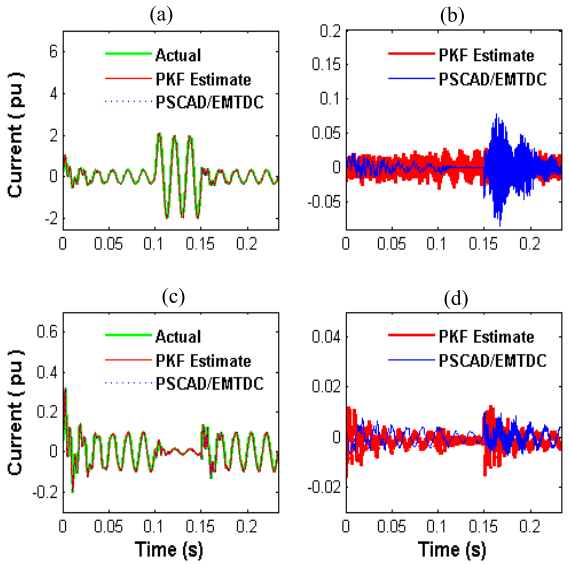

FIGURE 9. Actual, PKF estimation, PSCAD/EMTDC response of currents in transformer 5-6 and line 6-11, short circuit fault at busbar 6. (a) Transformer 5-6, (b) Residual, (c) Line 6-11, (d) Residual.

at the 7th cycle of the initial pre-fault period (cycles 1-6), followed by three cycles of fault condition (cycles 7-9), and then five cycles of post-fault state (cycles 10-14). The actual and PKF-PQSE estimates are in close agreement with the response obtained with PSCAD/EMTDC. NRMSE is 0.19% and 1.21%, respectively, for the PKF estimated currents, and 0.33% and 0.56% for PSCAD/EMTDC. Residuals have noticeable magnitudes during the post-fault period. However, the actual and estimated waveforms still present a close agreement.

Fig. 10 shows the generator current at busbars 1 and 2. The actual, PKF-PQSE estimate, and PSCAD/EMTDC response, respectively, closely agree. These generator currents fluctuate according with the transient short circuit condition at busbar 6. NRMSEs are 0.51% and 0.37% for PKF estimated currents, and 0.12% and 0.14% for currents obtained by PSCAD.

The residual fluctuations are constant during the period under analysis; only the PSCAD/EMTDC residual shows an increase in the post-fault period, but eventually disappears when the system steady state is reached.

D. PKF-PQSE UNDER A LOAD TRANSIENT CONDITION AT BUSBAR 14

The PQSE is assessed using the PKF considering a load transient at busbar 14 represented by the connection of a parallel resistive load at busbar 14 to simulate a sudden increment of electric load at the busbar. The connected resistive load is of 0.5 pu or 264.5 ohms; the load increase begins at the sixth cycle or 0.083 seconds and ends at the eleventh cycle or 0.167 seconds, the transient load condition remains active during five cycles.

Fig. 11 shows the actual and estimated waveforms for line currents and their difference during the state estimation.

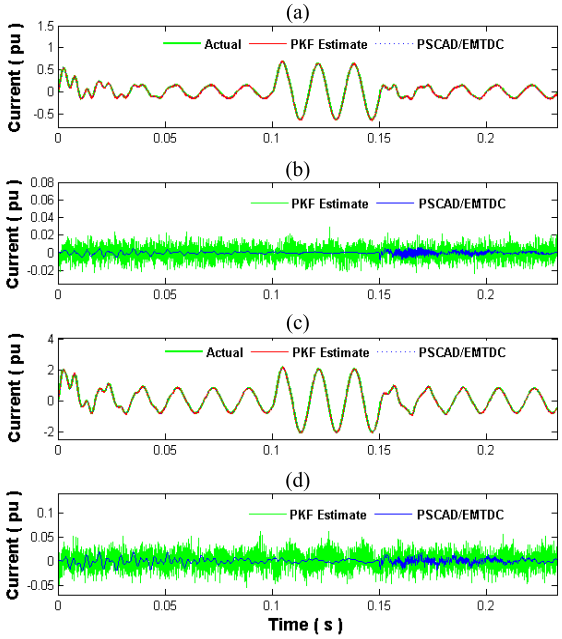

FIGURE 10. PKF-PQSE of generator currents at busbars 1-2, short circuit fault at busbar 6. (a) Generator busbar 1, (b) Residual, (c) Generator busbar 2, (d) Residual. The actual and estimated waveforms closely agree.

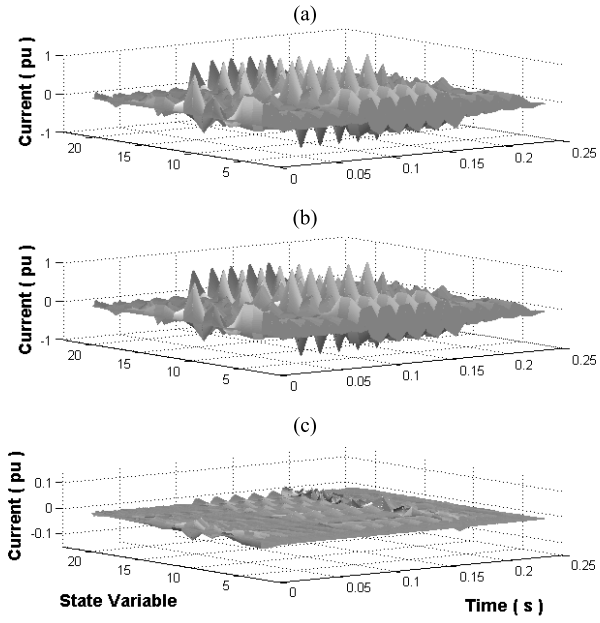

FIGURE 11. Actual, PKF estimate, and difference of line currents, load transient at busbar 14. (a) Actual, (b) PKF estimate, (c) Difference.

The difference is always below 5% and it is noticeable only during the transient load condition (6-10 cycles, 0.083-0.167 s) and when the load transient is removed (11 cycle). After the load transient, the power system reaches its steady state being the state estimation error or difference below 1.5% (after 11 cycle).

The load transient originates voltage and current fluctuations. Fig. 12 illustrates the waveforms for currents in

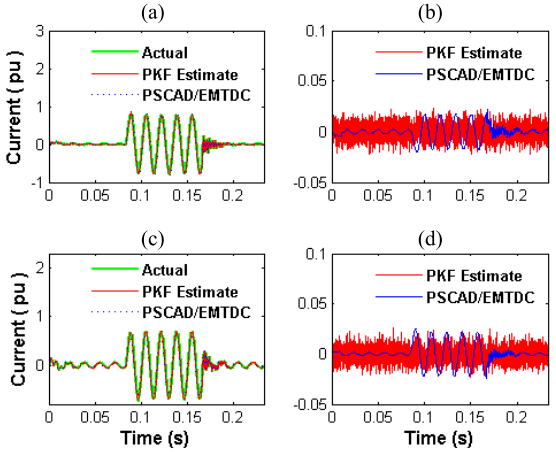

FIGURE 12. Actual, PKF estimate, PSCAD/EMTDC and residuals of currents in lines 9-14 and 13-14, load transient at busbar 14. (a) Line 9-14, (b) Residual, (c) Line 13-14, (d) Residual.

lines 9-14 and 13-14. The actual, estimated, and PSCAD/EMTDC waveforms are in close agreement during the state estimation (Figs. 12a and 12c); however, an error or residual is present, as shown in Figs. 12b and 12d.

The error between the actual waveform and the PKF-PQSE estimate is always below 2%, but the error between the actual waveform and the PSCAD/EMTDC response during the transient has a peak value of approximately 1.8% and after the transient, this error decays from 1.8% to less than 1% during the next two cycles, as shown in Fig. 12d. This error can be due to the measurement noisy condition during the state estimation and it does not depend of the integration method used. To obtain the actual system response, the RK4 and the trapezoidal rule (TR) methods were used, giving identical results. Therefore, an identical error was obtained when compared against the response obtained by the PSCAD/EMTDC simulator. The NRMSEs are 0.42% and 0.47% for the estimated currents in lines 9-14 and 13-14, respectively, during the 14 cycles under analysis.

Fig. 13 shows the generator currents at busbars 1 and 2. These waveforms show the load transient at busbar 14, beginning with the initial transient (1-3 cycles, 0.0-0.05 s), steady state period (4-5 cycles, 0.05-0.083 s), load transient (6-10 cycles, 0.083-0.166 s), post-load transient (11-13 cycles, 0.166-0.216 s), and periodic steady state (14 cycle, 0.216-0.233 s).

The actual, PKF-PQSE, and PSCAD/EMTDC responses are in close agreement during, after the load transient, and in the periodic steady state with a low state estimation error. The NRMSE between the actual and the PKF-PQSE is 0.66% and 0.42% for generator currents at busbars 1 and 2, respectively. Similarly, the NRMSE between actual and PSCAD/EMTDC response is 1.02% and 0.66% for the same generator currents.

Fig. 14 shows the estimated voltage at busbars 12, 13, and 14 using the PKF-PQSE method under the load transient. The voltage waveforms at busbars 12, 13, and 14 show a voltage sag during the load transient; approximately of 8, 10, and 20%

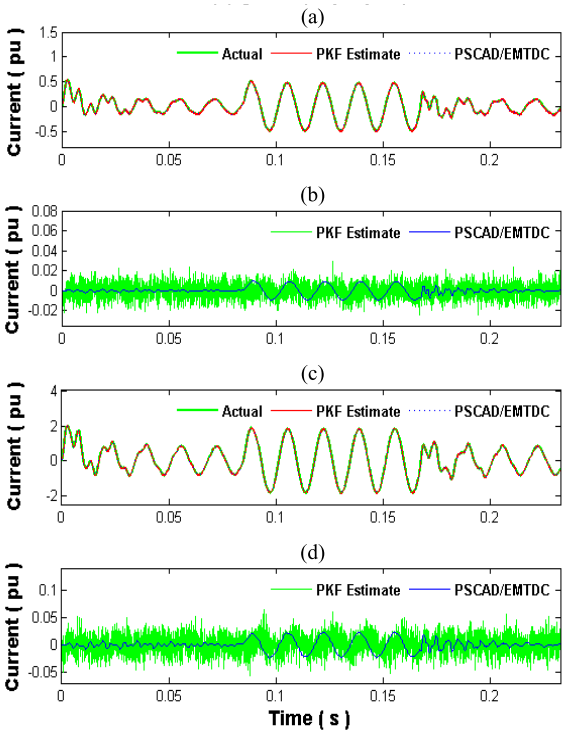

FIGURE 13. PKF-PQSE of generator currents at busbars 1-2, load transient at busbar 14. (a) Generator busbar 1, (b) Residual, (c) Generator busbar 2, (d) Residual. The maximum state estimation error is 1.02%.

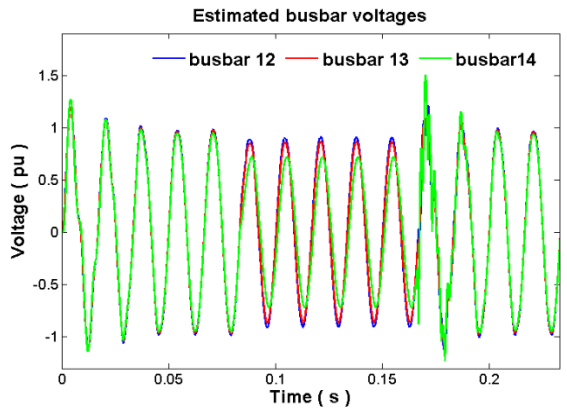

FIGURE 14. PKF-PQSE of voltages at busbars 12, 13, and 14 with transient condition at the electrical load of busbar 14. Voltage sag/swell condition is originated at the busbars.

respectively, and an increase of 10, 15, and 25% respectively, after the transient generating a voltage swell.

IV. CPU-GPU CHARACTERISTICS AND EXECUTION TIME

The PKF-PQSE method has been implemented on Intel(R) Xeon(R) CPU E5-1603, 2.8 GHz, 4 GB RAM jointly with Nvidia GeForce GT 630 GPU using C++, CUDA, and CUBLAS library. Table 6 gives the GPU characteristics.

The test system model was replicated several times to simulate and estimate systems with more state variables. Table 7 gives the number of replicated models, the number of states and the execution time for the sequential and parallel programs.

TABLE 6. Nvidia Geforce GT 630 GPU data.

Processor cores	384
GPU clock rate	902 MHz
Memory	2.0 GB
Memory clock rate	1.8 Gbps
Memory bus width	64 bit

TABLE 7. Execution time (s) and speed up.

Models	States	CPU C++ code	CPU-GPU Cublas	Normalized speed-up
1	43	26.54	5.02	0.264
2	86	323.49	13.84	1.168
3	129	1468.94	36.50	2.012
4	172	4413.77	73.48	3.003

TABLE 8. NRMSE results.

Case study	Generator current busbar	NRMSE % PKF-PQSE	NRMSE % Pscad/EMTDC
Variable harmonics	1	0.92	0.70
	2	0.53	0.68
Inter-harmonics	1	0.95	0.20
	2	0.53	0.20
Transients	1	0.51	0.12
	2	0.37	0.14

The normalized speed-up was calculated using (29) with a factor f_s of 20. The speed-up increases with the size of the electrical power grid. Parallel processing techniques based on the CPU-GPU configuration and the CUBLAS functions have been compared against the sequential execution of CPU C++ code. The case study of time-varying harmonics has been used to measure the execution times. From the obtained speed-up values, the PKF-PQSE method can be applied to obtain the time-domain state estimation assessment of large-scale power systems to reduce the execution time.

The PKF-PQSE takes less execution time than the CPU C++ sequential code to obtain the power system state as shown in Table 7. The PKF results have been compared against those obtained by the PSCAD/EMTDC simulator; the residuals indicate a close agreement between both responses.

A different comparison takes into account the NRMSE obtained by each case study. Table 8 shows results for current of generators at busbars 1 and 2. The maximum difference between the NRMSE of both solutions is approximately 0.75% for the generator current busbar 1 of the inter-harmonics case study.

The case studies show sudden variations in the time-varying harmonics, inter-harmonics, and transients, despite

of this, the PKF-PQSE methodology closely follows the fluctuations and adequately performs the time-domain state estimation.

The PKF-PQSE significantly speeds-up the state estimation in large-scale power systems, since the speed-up between the sequential and parallel execution is proportional to the number of states in the system. However, the PKF-PQSE requires the CPU-GPU configuration to apply parallel processing. This configuration needs data interchange between the CPU and GPU processors.

The nonlinear models of components and power systems can be analyzed and estimated by modifying the KF with extensions, such as the extended and unscented KFs. These filters can be implemented using parallel processing techniques on CPU-GPU systems to estimate nonlinear power system cases.

V. CONCLUSION

A time-domain state estimation method based on PKF (named PKF-PQSE) programmed using the CUDA platform and the CUBLAS library on GPU has been proposed. In particular, it has been applied for power systems with an underdetermined measurement equation and a significant number of state variables. The KF algorithm has been parallel implemented to assess the matrix operations to reduce the filter execution time. This parallel algorithm efficiently solves the time-domain state estimation of power systems considering time-varying harmonics, inter-harmonics, sub-harmonics, and electromagnetic transients. This state estimation has been evaluated with a reduced execution time and with an acceptable residual error according with the case studies results. The proposed PKF-PQSE methodology can be an attractive alternative to implement the real-time assessment of time-domain state estimation.

The PKF-PQSE method has been assessed in terms of computational efficiency in the GPU to show the obtained speed-up, as compared to the sequential execution to evaluate the time-domain state estimation (Table 7). For the analyzed case studies, the speed-up is proportional to the state variables of the system. The results obtained with the PKF-PQSE method have been successfully validated through direct comparison against the actual system response and against the PSCAD/EMTDC solution. In all cases, a close agreement was obtained. The average error between responses was 0.34%.

A set of first-order ordinary differential equations represents the dynamic response of the power system and its components. The estimated state variable waveforms have been obtained through the proposed time-domain methodology and their harmonic content through a DFT exercise. The PKF requires a power system model and a set of synchronized measurements from the system to estimate the state variables. The output variables are in turn calculated using the estimated state variables to be compared against the measured output variables to obtain the state estimation residual. A prospective work is to apply the CPU-GPU parallel processing system to assess the extended and unscented KFs state estimation in nonlinear power systems.

ACKNOWLEDGMENT

The authors gratefully acknowledge the Universidad Michoacana de San Nicolas de Hidalgo, Facultad de Ingeniería Eléctrica, División de Estudios de Posgrado (FIE-DEP) Morelia, Mexico, for the facilities granted to carry out this investigation.

REFERENCES

[1] J. Arrillaga, N. R. Watson, and S. Chen, *Power System Quality Assessment*. Hoboken, NJ, USA: Wiley, 2000.
[2] G. T. Heydt, *Electric Power Quality*, 2nd ed. West LaFayette, IN, USA: Stars in a Circle Publications, 1991.
[3] S. K. Jain and S. N. Singh, "Harmonics estimation in emerging power system: Key issues and challenges," *Electr. Power Syst. Res.*, vol. 81, no. 9, pp. 1754–1766, 2011, doi: 10.1016/j.epsr.2011.05.004.
[4] N. R. Watson, "Power quality state estimation," *Eur. Trans. Electr. Power*, vol. 20, no. 1, pp. 19–33, 2010, doi: 10.1002/etep.357.
[5] R. Cisneros-Magaña and A. Medina, "Time domain transient state estimation using singular value decomposition Poincare map and extrapolation to the limit cycle," *Electr. Power Energy Syst.*, vol. 53, pp. 810–817, Dec. 2013, doi: 10.1016/j.ijepes.2013.06.003.
[6] M. S. Grewal, A. P. Andrews, *Kalman Filtering: Theory and Practice Using MATLAB*. Hoboken, NJ, USA: Wiley, 2001.
[7] F. van der Heijden, R. P. W. Duin, D. de Ridder, and D. M. J. Tax, *Classification, Parameter Estimation and State Estimation*. Hoboken, NJ, USA: Wiley, 2004.
[8] M.-Y. Huang, S.-C. Wei, B. Huang, and Y.-L. Chang, "Accelerating the Kalman filter on a GPU," in *Proc. IEEE 17th Int. Conf. Parallel Distrib. Syst. (ICPADS)*, Dec. 2011, pp. 1016–1020, doi: 10.1109/ICPADS.2011.153.
[9] *NVIDIA: CUDA C Programming Guide, Version 5.0*, Nvidia Corp., Santa Clara, CA, USA, Oct. 2012.
[10] *NVIDIA: CUDA API Reference Manual, Version 5.0*, Nvidia Corp., Santa Clara, CA, USA, Oct. 2012.
[11] *NVIDIA: CUDA Toolkit 5.0 CUBLAS Library*, Nvidia Corp., Santa Clara, CA, USA, Apr. 2012.
[12] *NVIDIA: CUBLAS Library User Guide, Version 5.0*, Nvidia Corp., Santa Clara, CA, USA, Oct. 2012.
[13] H. M. Beides and G. T. Heydt, "Dynamic state estimation of power system harmonics using Kalman filter methodology," *IEEE Trans. Power Del.*, vol. 6, no. 4, pp. 1663–1670, Oct. 1991, doi: 10.1109/61.97705.
[14] J. Zhang, G. Welch, G. Bishop, and Z. Huang, "A two-stage Kalman filter approach for robust and real-time power system state estimation," *IEEE Trans. Sustainable Energy*, vol. 5, no. 2, pp. 629–636, Apr. 2014, doi: 10.1109/TSTE.2013.2280246.
[15] A. Medina and R. Cisneros-Magaña, "Time-domain harmonic state estimation based on the Kalman filter Poincare map and extrapolation to the limit cycle," *IET Generat., Transmiss. Distrib.*, vol. 6, no. 12, pp. 1209–1217, 2012, doi: 10.1049/iet-gtd.2012.0248.
[16] R. Cisneros-Magaña, A. Medina, and V. Dinavahi, "Parallel Kalman filter based time-domain harmonic state estimation," in *Proc. IEEE North Amer. Power Symp. (NAPS)*, Sep. 2013, pp. 1–6, doi: 10.1109/NAPS.2013.6666831.
[17] G. K. Singh, "Power system harmonics research: A survey," *Eur. Trans. Electr. Power*, vol. 1, no. 2, pp. 151–172, 2009, doi: 10.1002/etep.201.
[18] V. M. Moreno and A. Pigazo, *Kalman Filter: Recent Advances and Applications*. Vienna, Austria: InTech, 2009.
[19] G. Chang *et al.*, "Modeling devices with nonlinear voltage-current characteristics for harmonic studies," *IEEE Trans. Power Del.*, vol. 19, no. 4, pp. 1802–1811, Oct. 2004, doi: 10.1109/TPWRD.2004.835429.
[20] E. Acha and M. Madrigal, *Power Systems Harmonics Computer Modelling and Analysis*. Hoboken, NJ, USA: Wiley, 2001.
[21] A. Baggini, *Handbook of Power Quality*. Hoboken, NJ, USA: Wiley, 2008.
[22] G. A. Taylor, D. C. H. Wallom, S. Grenard, A. Y. Huete, and C. J. Axon, "Recent developments towards novel high performance computing and communications solutions for smart distribution network operation," in *Proc. IEEE PES Int. Conf. Exh. Innov. Smart Grid Technol. (ISGT Europe)*, Dec. 2011, pp. 1–8, doi: 10.1109/ISGTEurope.2011.6162812.

[23] V. Jalili-Marandi, Z. Zhou, and V. Dinavahi, "Large-scale transient stability simulation of electrical power systems on parallel GPUs," *IEEE Trans. Parallel Distrib. Syst.*, vol. 23, no. 7, pp. 1255–1266, Jul. 2012, doi: 10.1109/TPDS.2011.291.

[24] A. Medina, A. Ramos-Paz, and C. R. Fuerte-Esquivel, "Periodic steady state solution of electric systems with nonlinear components using parallel processing," *IEEE Trans. Power Syst.*, vol. 18, no. 2, pp. 963–965, May 2003, doi: 10.1109/TPWRS.2003.811166.

[25] Y. Chen and V. Dinavahi, "Multi-FPGA digital hardware design for detailed large-scale real-time electromagnetic transient simulation of power systems," *IET Generat., Transmiss., Distrib.*, vol. 7, no. 5, pp. 451–463, May 2013, doi: 10.1049/iet-gtd.2012.0374.

[26] Z. Liu, X. Geng, Z. Xie, and X. Lu, "The multi-core parallel algorithms of wavelet/wavelet packet transforms and their applications in power system harmonic analysis and data compression," *Int. Trans. Electr. Energ. Syst.*, vol. 25, pp. 2800–2818, Nov. 2015, doi: 10.1002/etep.1992.

[27] J. D. Owens, M. Houston, D. Luebke, S. Green, J. E. Stone, and J. C. Phillips, "GPU computing," *Proc. IEEE*, vol. 96, no. 5, pp. 879–899, May 2008, doi: 10.1109/JPROC.2008.917757.

[28] C. K. Chui and G. Chen, *Kalman Filtering With Real-Time Applications*. Berlin, Germany: Springer-Verlag, 2009.

[29] W. H. Press, S. A. Teukolsky, W. T. Vetterling, and B. P. Flannery, *Numerical Recipes in C: The Art of Scientific Computing*, 2nd ed. Cambridge, U.K.: Cambridge Univ. Press, 1992.

[30] S. Tomov, R. Nath, H. Ltaief, and J. Dongarra, "Dense linear algebra solvers for multicore with GPU accelerators," in *Proc. IEEE Int. Symp. Parallel Distrib. Process., Workshops Phd Forum (IPDPSW)*, Apr. 2010, pp. 1–8, doi: 10.1109/IPDPSW.2010.5470941.

[31] H. El-Rewini and M. Abd-El-Barr, *Advanced Computer Architecture and Parallel Processing, Wiley Series on Parallel and Distributed Computing*. Hoboken, NJ, USA: Wiley, 2005.

[32] I. Foster, *Designing and Building Parallel Programs: Concepts and Tools for Parallel Software Engineering*. Reading, MA, USA: Addison-Wesley, 1995.

[33] J. Nickolls and W. J. Dally, "The GPU computing era," *IEEE Micro*, vol. 30, no. 2, pp. 56–69, Apr. 2010, doi: 10.1109/MM.2010.41.

[34] V. Volkov and J. W. Demmel, "Benchmarking GPUs to tune dense linear algebra," in *Proc. IEEE SC Int. Conf. High Perform. Comput., Netw.*, Jun. 2008, pp. 1–11, doi: 10.1109/SC.2008.5214359.

[35] *IEEE 14 Bus Test System, Power Systems Test Case Archive*. Accessed: Feb. 15, 2018. [Online]. Available: https://www2.ee.washington.edu/research/pstca/pf14/pg_tca14bus.htm

[36] R. C. Dugan, M. F. McGranaghan, S. Santoso, and H. W. Beaty, *Electrical Power Quality*, 2nd ed. New York, NY, USA: McGraw-Hill, 2002.

[37] N. Watson and J. Arrillaga, *Power Systems Electromagnetics Transients Simulation*, 2nd ed. London, U.K.: The Institution of Engineering and Technology, 2007.

[38] W. G. Morsi and M. E. El-Hawary, "Power quality evaluation in smart grids considering modern distortion in electric power systems," *Electr. Power Syst. Res.*, vol. 81, no. 5, pp. 1117–1123, 2011, doi: 10.1016/j.epsr.2010.12.013.

[39] M. H. J. Bollen, P. Ribeiro, I. Y. H. Gu, and C. A. Duque, "Trends, challenges and opportunities in power quality research," *Eur. Trans. Electr. Power*, vol. 20, no. 1, pp. 3–18, 2010, doi: 10.1002/etep.370.

[40] Y. Wang, H. E. Mazin, W. Xu, and B. Huang, "Estimating harmonic impact of individual loads using multiple linear regression analysis," *Int. Trans. Electr. Energ. Syst.*, vol. 26, no. 4, pp. 809–824, 2016, doi: 10.1002/etep.2109.

[41] A. Testa *et al.*, "Interharmonics: Theory and modeling," *IEEE Trans. Power Del.*, vol. 22, no. 4, pp. 2335–2348, Oct. 2007, doi: 10.1109/TPWRD.2007.905505.

[42] E. W. Gunther, "Interharmonics in power systems," in *Proc. IEEE Power Eng. Soc. Summer Meeting*, vol. 2. Jul. 2001, pp. 813–817, doi: 10.1109/PESS.2001.970156.

[43] *Pscad User's Guide, Version 4.2.0*, Manitoba HVDC Research Centre Inc., Winnipeg, Canada, 2005.

RAFAEL CISNEROS-MAGAÑA (S'07–M'13) received the M.Sc. and Ph.D. degrees in electrical engineering from the Facultad de Ingeniería Eléctrica, Universidad Michoacana de San Nicolás de Hidalgo, Morelia, México, in 2009 and 2013, respectively.

His current research interests include the modeling, analysis, and simulation of power systems, time domain state estimation, power quality adverse phenomena, and renewable energy systems, including wind and photovoltaic generation, power electronics and electromagnetic transients, and numerical parallel processing applied to power system simulation.

AURELIO MEDINA (SM'02) received the Ph.D. degree from the University of Canterbury, Christchurch, New Zealand, in 1992. He was a Post-Doctoral Fellow at the Universities of Canterbury, New Zealand (one year) and Toronto, ON, Canada (two years).

He joined the Facultad de Ingeniería Eléctrica, Universidad Michoacana de San Nicolás de Hidalgo, Morelia, México, in 1995. His research interests are in the analysis of power quality phenomena, dynamic and steady state analysis of power systems, renewable energy systems, and the application of advanced numerical and computer techniques to power system analysis.

VENKATA DINAVAHI (S'94–M'00–SM'08) received the Ph.D. degree in electrical and computer engineering from the University of Toronto, in 2000.

He is currently a Professor with the University of Alberta. His research interests include real-time simulation of power systems and power electronic systems, large-scale system simulation, and parallel and distributed computing.

ANTONIO RAMOS-PAZ was born in Morelia, México, in 1975. He received the B.Sc. degree in electrical engineering and the M.Sc. and Ph.D. degrees from the Universidad Michoacana de San Nicolás de Hidalgo, Morelia, in 2001, 2002, and 2007, respectively.

He is currently an Associate Professor with the División de Estudios de Posgrado, Facultad de Ingeniería Eléctrica, Universidad Michoacana de San Nicolás de Hidalgo. His research interests include power systems analysis and modeling, as well as techniques of parallel processing.